World Electric Vehicle Journal

MDPI

Article

Research on Road Sense Simulation Control of Steering-by-Wire Based on Sliding Mode Control

Suojun Hou [1,2], Kang An [1,*], Zhu An Zheng [1], Yaning Qin [1] and Qichang Xie [1]

[1] School of Automotive Engineering, Yancheng Institute of Technology, Yancheng 224051, China
[2] School of Vehicle and Traffic Engineering, Henan Institute of Technology, Xinxiang 453000, China
* Correspondence: 15038649621@163.com

Abstract: To enhance the driving experience for drivers, making it more realistic and comfortable, this study proposes a simulation control strategy for steering-by-wire road sense based on sliding mode control. Firstly, a dynamic model is constructed for the steering wheel module and the steering actuator, building upon this, a methodology for calculating the self-aligning torque is formulated, utilizing the linear two-degree-of-freedom vehicle model in conjunction with the Magic Formula. The approach incorporates the influences of assistive forces, damping, and frictional torque, thereby providing an accurate simulation of the steering road feel. On this basis, a sliding mode control algorithm is developed to achieve the necessary road-sensing motor current, guaranteeing system stability and rapid response across various driving scenarios. To validate the simulation, MATLAB/Simulink in conjunction with Carsim is employed. The outcomes from tests involving dual lane shifts and step inputs demonstrate that the introduced control approach effectively follows the target current, featuring swift convergence and minimal response latency.

Keywords: steer-by-wire; road sense simulation; sliding mode control; magic formulas; current control

check for updates

Academic Editor: Michael Fowler

Received: 10 February 2025
Revised: 10 March 2025
Accepted: 14 March 2025
Published: 16 March 2025

Citation: Hou, S.; An, K.; Zheng, Z.A.; Qin, Y.; Xie, Q. Research on Road Sense Simulation Control of Steering-by-Wire Based on Sliding Mode Control. *World Electr. Veh. J.* **2025**, *16*, 175. https://doi.org/10.3390/wevj16030175

Copyright: © 2025 by the authors. Published by MDPI on behalf of the World Electric Vehicle Association. Licensee MDPI, Basel, Switzerland. This article is an open access article distributed under the terms and conditions of the Creative Commons Attribution (CC BY) license (https://creativecommons.org/licenses/by/4.0/).

1. Introduction

As automotive technology advances swiftly, steer-by-wire (SBW) is recognized as one of the mainstream options for future steering systems, which improves driving mobility, makes the interior space more flexible, facilitates the integration of intelligent driving unit control, and is a key technology of autonomous vehicles [1]. Steering-by-wire systems use technologies such as drive motors, electronic controls, and sensors, which are replacing the traditional mechanical connection between the steering wheel and the wheels, resulting in road sense information not being passed on to the driver. Hence, supplementary feedback motors for road-sensing are necessary to convey authentic data to the driver regarding the front wheels' engagement with the pavement [2].

A great deal of work has been conducted on SBW system control in order to obtain realistic road sense feedback moments. Fankem et al. [3] proposed a rack and pinion force-based design of road-sensing feedback torque control strategy, while the modular design of each part can meet the needs of drivers with different driving styles. In addition, Kirli et al. [4] used a steering hysteresis model-based optimization of the SBW system, which was validated by hardware-in-the-loop tests to achieve adaptive optimization of hysteresis parameters to dynamically adjust the steering feedback. However, due to the limitations of the model, satisfactory control performance could not be obtained. Cheon et al. [5] developed a control module for the steering wheel assembly within the SBW system to enhance the actuator's performance for steering road-sensing. To bolster the module's robustness, a

compensator control algorithm incorporating inertia and friction compensation was crafted to guarantee the accuracy of the road-sensing torque feedback. Zhang et al. [6] proposed a linear self-resilient control strategy based on a differential evolutionary algorithm that ensures smoother driving sensation and real-time road perception. However, the response time is delayed due to the self-tuning to find the optimal controller parameters, which should be dealt with. Gholami et al. [7] used a linear two-degree-of-freedom model to design a Kalman filter to predict the lateral force exerted by the tires and further calculate the upper moment of the steering wheel, which was verified to be highly accurate. At the same time, Van Ende et al. [8] trained, analyzed, and evaluated different network topologies, and the results show that Artificial Neural Networks (ANNs) have basic applicability in simulating steering torque, providing a new solution for the control of an SBW system.

In terms of road sense analogue motor control, Liang et al. [9] introduced an adaptive friction torque compensation control system, which is used to improve the tracking accuracy by processing and estimating the friction parameters through a LuGre observer and is physically verified to have both high compensation tracking accuracy and robustness. WeiHe L et al. [10] developed a current harmonic control approach utilizing an extended Kalman filter algorithm, which is experimentally verified to be robust to nonlinear systems and capable of suppressing currents in all frequency ranges. Yu L et al. [11] used an integral sliding mode controller to obtain convergence of the state error. Roman M et al. [12] used a grey-box model to identify the SBW system parameters and tracked the reference signal using a linear quadratic regulator (LQR) and an all-state system observer, and the experimental findings indicate that the approach not only enhances system robustness, but also optimizes the control performance, especially in the face of parameter variations and external perturbations, and still has a high accuracy. Zhe S et al. [13] developed an adaptive sliding mode controller to address uncertainties and nonlinear factors in the system and adjusted the controller in real time, and it was verified that the adaptive sliding mode controller has good tracking results. Ye M et al. [14] put forth an adaptive terminal sliding mode controller that utilizes the Extreme Learning Machine (ELM) algorithm, which was verified by numerical simulation and not only improved the convergence of the error, but also effectively estimated the uncertainty of the system. Wang H [15] proposes a robust neural network-based control system using radial basis function neural networks to adaptively learn the uncertainty boundaries in Lyapunov's sense, which effectively removes the effect of uncertainty in a closed-loop system. Wang H [16] proposed a novel vehicle stability control (VSC) with a combination of upper yaw rate controller and lower steering controller design to realize the accurate tracking of yaw rate and steering angle. The simulation results show that the proposed VSC scheme has good stability and robustness. Liu [17] proposed a road-sensing construction scheme using steering feedback torque (SFT) controller with convolutional neural network and friction explicit model predictive control (FEMPC), and simulation and experimental results showed that the scheme has high reliability and accuracy. Chen Y [18] proposed a torque feedback model and further determined the parameters of the road sense simulation function by analyzing the characteristics of the steering torque resistance, which was verified by the test rig. Hang P [19] designed a fast terminal sliding mode controller with an extended Kalman filter to estimate the side deviation angle, and the simulation results show that the controller has better tracking capability and strong robustness. Lee J [20] proposed a haptic control system for tracking the target torque using adaptive sliding mode to ensure robustness to parameter uncertainties, and the proposed controller was verified by simulation to be capable of being able to track the target torque. Lee S [21] designed the force feedback unit and verified its algorithm to be effective through modelling. Su C R [22] proposed a personalized steering feel model using an extended perturbation observer to estimate

the rack force and calculate the friction moment as well as the power assist to introduce variable parameters to design personalized steering feel for different populations.

Given the aforementioned considerations, researchers have used different methods to achieve a simulation of the road-sensing torque to some extent or have used various control algorithms to control the current accurately in order to arrive at an accurate control of the torque magnitude. However, there is still limited research in optimizing the road-sensing torque algorithm and coordinating the control of road-sensing motors at the same time. Therefore, in this paper, a sliding mode control-based road-sensing simulation controller is designed for automotive road-sensing simulations, and the effects of various strategies on the motor current are also investigated. The main contents of this paper are reflected in the following aspects.

1. Aiming at the inaccuracy and oscillation of the road-sensing moment, the source of road-sensing is analyzed, and the kinetics is used to model the back-correcting moment by combining the Magic Formula and the linear two-degree-of-freedom vehicle model, based on which the power-assisted characteristic curves of electric power steering vehicles are added, and auxiliary moments and damping moments are added to simulate real road-sensing.
2. To improve the response speed of the system and reduce current oscillations, a sliding mode control (SMC) strategy is used to ensure that the current converges in a finite period of time. The SMC also tracks the road-sensing to simulate the motor currents. The performance of the controller is verified by comparing and evaluating it with a PI controller and a fuzzy PID controller under different operating conditions.

2. Dynamic Modelling of Systems

In order to analyze the system, it is necessary to develop a model of the system dynamics, and the dynamic model of the steer-by-wire system that is developed in this study is displayed in Figure 1.

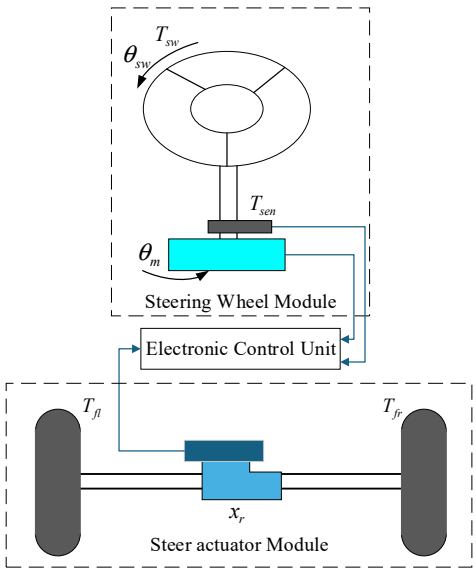


Figure 1. Dynamic model of steer-by-wire.

The system consists of two primary parts: the steering wheel assembly and the steering actuator assembly. Its core components include the steering disc, corner torque sensor, road-sensing analogue motor, steering actuator motor, electronic control unit, and rack and pinion steering gear.

The meaning of the symbols in Figure 1 is as follows: T_{sw} is the steering wheel input torque, θ_{sw} is the steering wheel angle, θ_m is the road sense analogue motor output angle, T_{sen} is the value of the torque measured by the sensor, and T_{fl} and T_{fr} are the return torque of the left and right front wheels x_r is the rack displacement.

2.1. Steering Wheel System

When the driver turns the steering wheel, the dynamics equations are formulated by treating the steering wheel and steering column as a unified component [23].

$$T_{sw} = J_{sw}\theta_{sw} + B_{sw}\theta_{sw} + T_{sen} + T_c \tag{1}$$

$$T_{sen} = k_s(\theta_{sw} - \theta_m / G_m) \tag{2}$$

where J_{sw} is the coefficient of inertia of the steering column, B_{sw} is the damping coefficient of the steering column, T_c is the friction torque of the steering wheel assembly, k_s is the stiffness of the steering column, and G_m is the reduction ratio of the road-sensing analogue motor.

The balance equation for the road-sensing analogue motor to the steering column via the reducer is as follows:

$$T_a = J_m d^2\theta / dt^2 + B_m d\theta / dt - T_{sen} / G_m \tag{3}$$

where T_a is the output torque of the road-sensing motor, and J_m and B_m are the rotational inertia and damping coefficient of the road-sensing motor.

Based on Kirchhoff's law, the interplay among motor voltage, current, resistance, and inductance is described by the following relationship [24]:

$$U_a = R_a I_a + L_a dI_a / dt + k_a d\theta_m / dt \tag{4}$$

where U_a is the motor input voltage, R_a is the motor resistance, I_a is the motor current, L_a is the motor inductance, and k_a is the motor reverse electromotive force coefficient.

The road-sensing analogue motor's output torque and operating current are as follows:

$$T_a = k_i I_a \tag{5}$$

where k_i is the road sense analogue motor torque coefficient.

2.2. Steering Actuator System

In the process of steering, the dynamic equations of the rack and pinion steering mechanism are as follows:

$$M_r d^2 x_r / dt^2 + B_r dx_r / dt + F_{rack} = \frac{k_{sa}(\theta_{sa} / G_{sa} - x_r / r_p)}{r_p} \tag{6}$$

$$F_{rack} = \frac{T_{fl}}{l_{fl}} + \frac{T_{fr}}{l_{fr}} \tag{7}$$

where M_r is the rack and pinion mass, B_r is the rack and pinion damping coefficient, F_{rack} is the rack and pinion force acting on the rack and pinion by the left and right tie rods, θ_{sa} is the turning angle of the steering actuator motor, G_{sa} is the reduction ratio of the steering actuator motor reducer, r_p is the steering pinion radius, and l_{fr} and l_{fr} are the length of the left and right front wheel steering rocker arms.

2.3. Two-Degree-of-Freedom (TDF) Vehicle Model

For a linear 2-TDF model, the vehicle's steering stability is commonly assessed through yaw velocity and side acceleration, as indicated in reference [25]. The model representing this 2-TDF vehicle dynamics is depicted in the accompanying Figure 2.

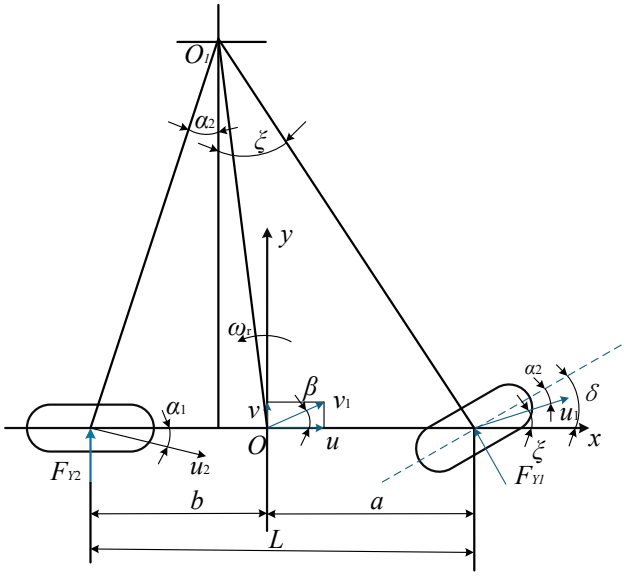


Figure 2. Two-degree-of-freedom vehicle model.

Force analysis conducted for the 2-TDF vehicle model is as follows:

$$F_{Y1}\cos\delta + F_{Y2} = m(dv/dt + \omega_r) \tag{8}$$

$$aF_{Y1}\cos\delta - bF_{Y2} = I_z d\omega_r/dt \tag{9}$$

where F_{Y1} and F_{Y2} are the front and rear axle lateral force, δ is the front wheel angle, m is the mass of the vehicle, v is the lateral velocity, u is the longitudinal velocity, I_z is the rotational inertia of the vehicle around the z-axis, and ω_r is the pendulum angular velocity.

The side deflection angles of the front and rear wheels are as follows:

$$\alpha_1 = \beta + \frac{a\omega_r}{u} - \delta \tag{10}$$

$$\alpha_2 = \beta - \frac{b\omega_r}{u} \tag{11}$$

where α_1 and α_2 are the front and rear wheel side deflection angle, β is the side slip angle, a is the distance from the centre of mass to the front axle, and b is the distance from the centre of mass to the rear axle.

3. Road Sense Feedback Torque Design

This study uses kinetic modelling to design the road sense feedback torque. The road sense feedback torque is analyzed and the booster characteristic is added to make steering easier, while the damping and friction torques are added to compensate for them.

3.1. Calculation of Self-Aligning Torque

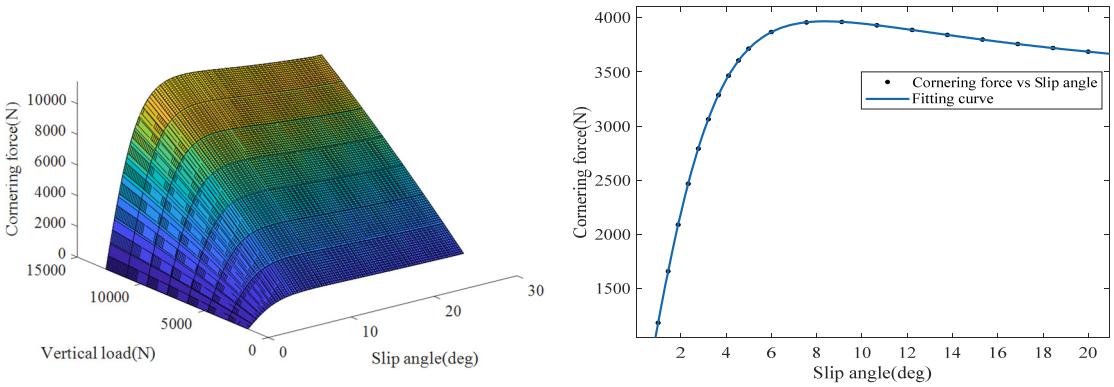
To examine the impact of tire side deflection properties on the steering wheel self-returning torque during the steering process of automobiles, the magic tire model is established. The Magic Formula, derived from test data, offers high accuracy within the tested range, where even outside the limit value of a certain degree can still be used.

This study uses the Magic Formula tire model [26]. The Magic Formula of the sinusoidal expression is as follows:

$$Y(x) = D\sin\{\text{Carctan}[Bx - E(Bx - \arctan(Bx))]\} \tag{12}$$

where x is the tire's lateral deflection angle, the output is the lateral force or aligning torque, and B, C, D, E are the influence factors.

To solve this problem, we used custom equations from the MATLAB/Cftool toolbox suite to estimate the parameters of the coefficients in the Magic Formula. As shown in Figure 3, a plot shows the raw Carsim lateral force data and b plot shows the results of fitting the lateral force under vertical loading on the front axle of the selected model. Table 1 details the parameters of the selected model.



(**a**) (**b**)

Figure 3. Lateral force characteristic diagram: (**a**) lateral force 3D plot; (**b**) lateral force fitting results.

Table 1. Vehicle parameters.

Symbol	Value	Unit
m	1270	kg
I_z	1536.7	kg·m^2
k_1	−58,058.06	N/rad
k_2	−31,092.4	N/rad
a	1.015	m
b	1.895	m

The fitting results are as follows:

$$B = 0.2162, C = 1.4122, D = 3966.9, E = -0.2863$$

To avoid repeating the description, the lateral forces on the rear axle tires are the same.

By combining Formulas (8)–(12), a nonlinear TDF model is established and the self-aligning torque are fitted, as shown in Figure 4.

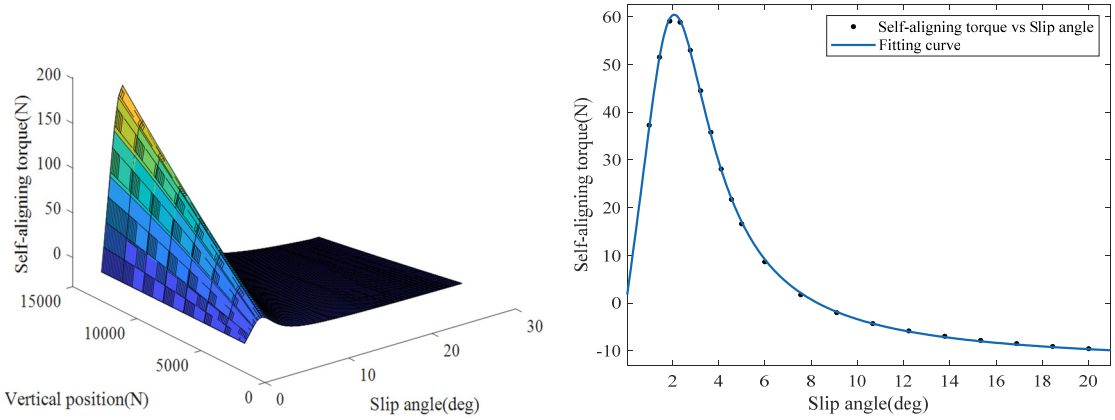
Similarly, the self-aligning torque were fitted, and the fitted values are as follows:

$$B = -0.2726, C = 2.1456, D = -60.4259, E = -6.4257$$

To ensure the precision of the estimated parameters within a nonlinear vehicle dynamics model that encompasses TDF, one can employ the coefficient of determination, often denoted as R-squared.

$$R^2 = 1 - \frac{SSE}{SST} \tag{13}$$

where SSE is the residual sum of squares, and SST is the total sum of squares.



(**a**) (**b**)

Figure 4. Three-dimensional diagram of self-aligning torque characteristics: (**a**) self-aligning torque 3D plot; (**b**) self-aligning torque fitting results.

The fitting effects of the lateral force and self-aligning moment of the front and rear tires are shown in Table 2, in which the larger value of SSE of the front wheel is caused by the too large value near the fitting point, the RMSE of all three are smaller, and the R-square and Adjusted R-square are close to 1, which is a good fitting effect. It is verified that the Magic Formula used in this study is highly accurate and effectively describes the tire's side bias characteristics.

Table 2. Parameter goodness of fit.

Name	Front Axle Tire	Rear Axle Tire	Self-Aligning Torque
SSE	42.233	13.001	1.9903
R-square	0.9999	0.9999	0.99984
Adjusted *R*-square	0.9999	0.9999	0.99986
RMSE	1.6266	0.90142	0.3527

3.2. Assist Torque Design

The EPS steering system is analyzed and, based on the obtained right and left wheel return torque of the front axle, is conveyed to the steering column through the action of the transmission ratios, noted as T_{co}. In the EPS system, ECU modulates the assist torque based on the booster characteristic curve, considering the vehicle's velocity and the torque applied to the steering wheel. This process is crucial for adjusting the steering effort to ensure driver comfort and vehicle stability. As detailed in the research, a curvilinear power assist characteristic curve is employed for this purpose. The specific characteristic curve utilized in this context is depicted in Figure 5 [27].

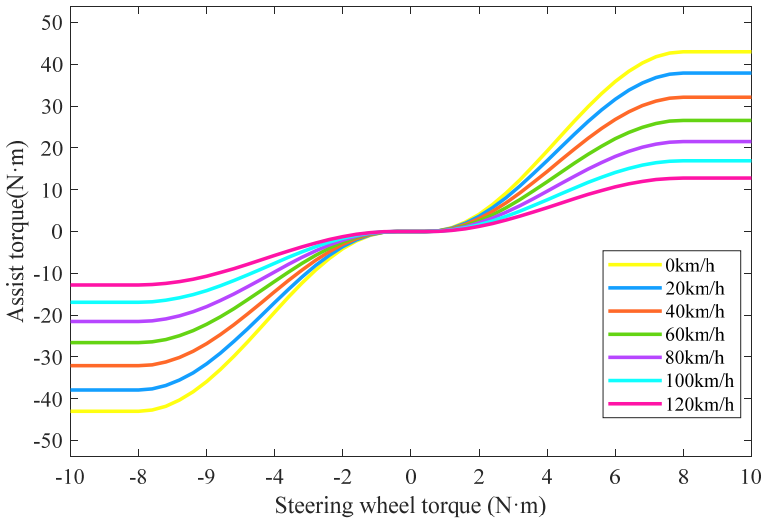


Figure 5. Power assist characteristic curve.

3.3. Design of Damping and Friction Torque

Damping and friction torque were designed to mitigate vehicle instability resulting from the driver's rapid steering wheel rotations at high speeds and to enhance the precision of steering wheel return when reversing direction [28]. Damping control does not work at low speeds, and at high speeds it is linearly related to the steering wheel angle.

$$T_{damp} = \begin{cases} 0 & v < v_1 \\ k_{damp}(v - v_1) & v \geq v_1 \end{cases} \tag{14}$$

where T_{damp} is the damping torque, k_{damp} is the damping torque coefficient, and v_1 is the minimum speed threshold for the action of the damping torque.

SBW technology cancels the physical linkage between the steering input and the actuation components, and the frictional torque decreases and needs to be compensated for.

$$T_{fic} = k_{fic} \cdot \tanh(c \cdot d\theta_{sw}/dt) \tag{15}$$

where T_{firc} is the frictional torque; k_{firc} is the frictional torque coefficient; and c is the adjustment factor.

The final road sense feedback torque is as follows:

$$T_{road} = T_{co} - T_a + T_{damp} + T_{firc} \tag{16}$$

3.4. Simulation Tests

Among the SBW simulation models, the steering wheel module and the steering actuation model are established in MATLAB/Simulink instead of the respective components in the Carsim vehicle dynamics model, and the viability of the road sense feedback torque in the SBW co-simulation is verified through the tests of dual lane/single lane transformation, central steering, etc. Owing to constraints on space paper, only the outcomes of the double lane change analysis are displayed. For velocities below 30 km/h, the lateral swing angular velocity, side acceleration, and steering wheel torque data are derived from both the SBW joint simulation model and the Carsim model, as illustrated in Figure 6. The results from the tests reveal that the corresponding parameters' response curves exhibit minor deviations, adequately addressing the requirements for steering road feedback and laying the groundwork for the control of motor currents in road-sensing applications.

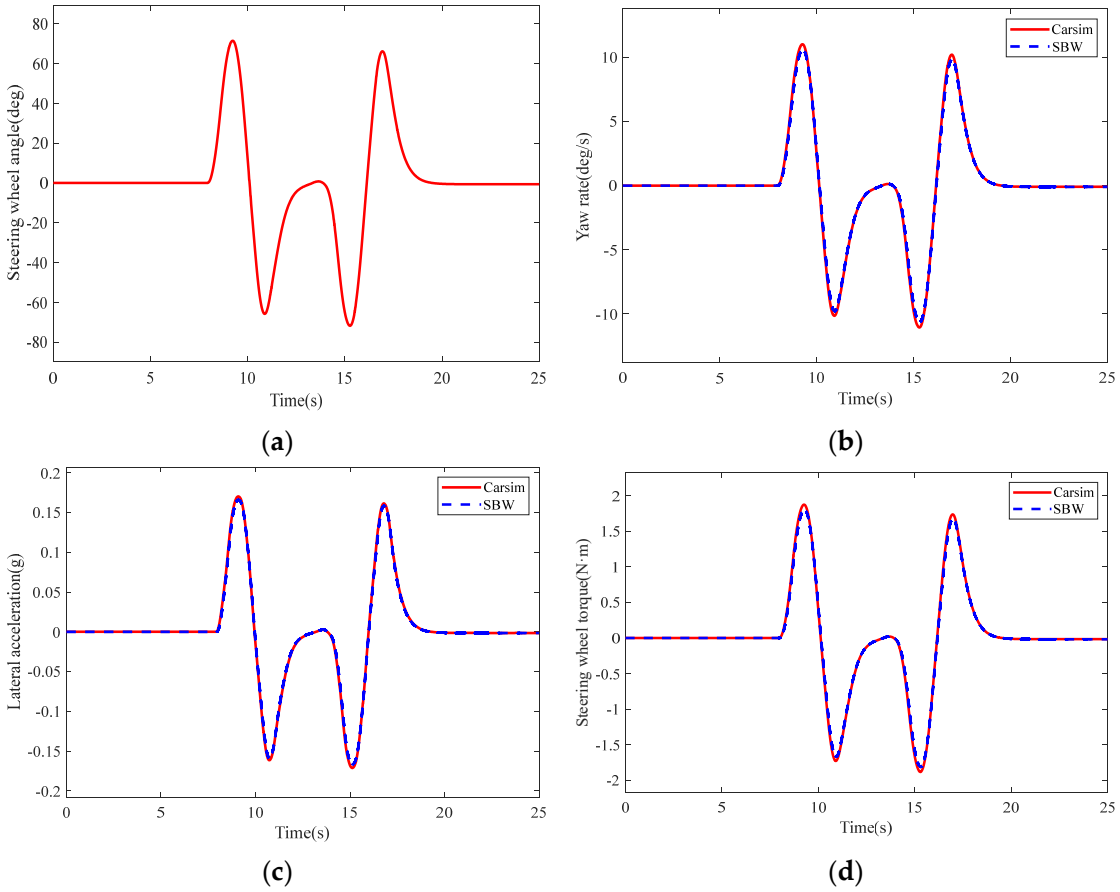


Figure 6. Comparison between SBW model and Carsim model: (**a**) steering wheel angle; (**b**) yaw rate comparison; (**c**) lateral acceleration comparison; (**d**) steering wheel torque comparison.

4. PID and SMC Strategy

In order to duplicate the same road feel as EPS, reduce current fluctuations, and accurately track the expected current, it is essential to set up relative control strategies to bring the steering system to the desired state. The schematic representation of the overarching control strategy developed in this study is presented in Figure 7. As depicted in Figure 7, upon the driver's steering wheel angle input, the discrepancy between the ideal and actual rack displacement is calculated. Subsequently, PID control is applied to direct the front wheel steering. Concurrently, the front wheel angle, vehicle speed, and steering wheel torque are fed into the road sense torque to ascertain the target current for the road-sensing simulation motor. In parallel, the SMC module swiftly drives the target current to emulate the actual road-sensing. This section outlines the design of the hierarchical strategy's control components.

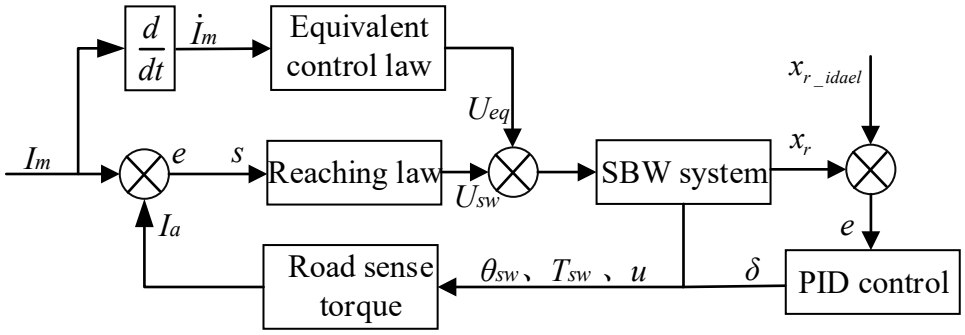


Figure 7. General control strategy.

4.1. PID Control Strategy

When steering the front wheels, the rack displacement serves as the control parameter, with the steering wheel angle deviation from the target rack and pinion position to the actual rack displacement being translated into PID control signals.

Desired rack displacement is as follows:

$$x_{r_ideal} = C\ Factor \times \frac{\delta_{sw}}{360^\circ} \tag{17}$$

where *C Factor* is the total displacement of the rack when the steering wheel rotates one revolution, and takes the value of 44.12 mm/rev.

4.2. Design of Sliding Mode Controller

Considering the reduction ratio of the road-sensing motor, combined with Equation (5), the target current is obtained as follows:

$$I_m = \frac{T_{road}}{G_m k_i} \tag{18}$$

Therefore, the tracking error between the designed target current and the actual current of the road sensor motor is as follows:

$$e = I_m - I_a \tag{19}$$

Let $s = e$ and combine with Equation (9) to obtain the derivative of s.

$$ds/dt = dI_m/dt - \frac{u - R_a I_a - k_a d\theta_m/dt}{L_a} \tag{20}$$

Let $ds/dt = 0$, we obtain the following:

$$U_{eq} = L_a dI_m/dt + R_a I_a + k_a d\theta_m/dt \tag{21}$$

where U_{eq} is the equivalent control term.

The expression uses an exponential convergence law [29].

$$ds/dt = -\varepsilon \mathrm{sgn}(s) - ks \tag{22}$$

where ε is the convergence velocity, $\varepsilon > 0$, $k > 0$.

Then, the switching term is as follows:

$$U_{sw} = L_a[\varepsilon \mathrm{sgn}(s) + ks] \tag{23}$$

The expression for the sliding mode controller is provided as follows:

$$U_a = L_a dI_m/dt + R_a I_a + k_a d\theta_m/dt + L_a[\varepsilon \mathrm{sgn}(s) + ks] \tag{24}$$

4.3. Closed-Loop Stability Analysis

For SBW systems with error dynamics, the control law used is as follows:

$$U = U_{eq} + U_{sw} \tag{25}$$

The requisite tracking error is then asymptotically driven to zero within a bounded time interval, thereby ensuring the system's trajectory closely aligns with the prescribed path.

To illustrate the reliability of the developed control algorithm, the Lyapunov function is formulated as follows:

$$V(s) = \frac{s^2}{2} \tag{26}$$

The derivation of s is obtained as follows:

$$\begin{aligned} dV/dt &= sds/dt \\ &= s(dI_m/dt - \tfrac{u - R_a I_a - k_a d\theta_m/dt}{L_a}) \\ &= s[-\varepsilon \mathrm{sgn}(s) - ks] \\ &= -\varepsilon|s| - ks^2 \\ &\leq 0 \end{aligned} \tag{27}$$

When $dV/dt \equiv 0$, $s \equiv 0$, based on the Lassalle invariance principle, the control system will tend to stabilize. Obviously, the closed-loop dynamic error can converge to the sliding mode surface.

To curtail system oscillations, a saturation function is used instead of a sign function.

$$sat(s) = \begin{cases} \mathrm{sgn}(s) & |s| > \Delta \\ ks & |s| < \Delta \end{cases} \tag{28}$$

where $k = \frac{1}{\Delta}$, Δ is called the boundary layer.

The expression for the final sliding mode controller is as follows:

$$U_a = L_a dI_m/dt + R_a I_a + k_a d\theta_m/dt + L_a[\varepsilon \mathrm{sat}(s) + ks] \tag{29}$$

5. Simulation Test

This study verifies the accuracy of the road-sensing simulation algorithm and examines the practicality and benefits of the control strategy by performing Carsim/Simulink co-simulation, comparing the results with those of the PI controller and the fuzzy PID controller.

5.1. Double Lane Change Test Conditions

The road friction coefficient is 0.85. The vehicle speed is set to 30 km/h and 80 km/h to verify the effectiveness of the controller at low and high speeds, the steering wheel angle is set to double lane input, and the tracking effect of the motor currents under the different algorithms is shown in Figure 8.

From Figure 8, it can be seen that the current tracking under fuzzy PID is better than PI control and the motor does not work in the dead zone position, but compared with the slip mode controller, the SMC has better performance, faster convergence, smaller error, and shorter response time. Tables 3 and 4 show the comparison of current performance metrics of the controller at 30 km/h and 80 km/h, respectively.

From Tables 3 and 4, it can be seen that the maximum error is 1.9% with PI control, the maximum error of fuzzy PID is 0.49%, while with sliding mode controller, the maximum error is significantly reduced, and the convergence speed is faster.

Table 3. Double shift lane response performance metrics at 30 km/h.

Name	SMC	PI	Fuzzy PID
Maximum current (A)	3.5	3.478	3.496
Maximum error (A)	0.0003	0.0453	0.0135
Maximum deviation (%)	0.09	1.294	0.38

Table 4. Double shift lane response performance metrics at 80 km/h.

Name	SMC	PI	Fuzzy PID
Maximum current (A)	7.8747	7.508	7.891
Maximum error (A)	0.0168	0.152	0.038
Maximum deviation (%)	0.21	1.9	0.49

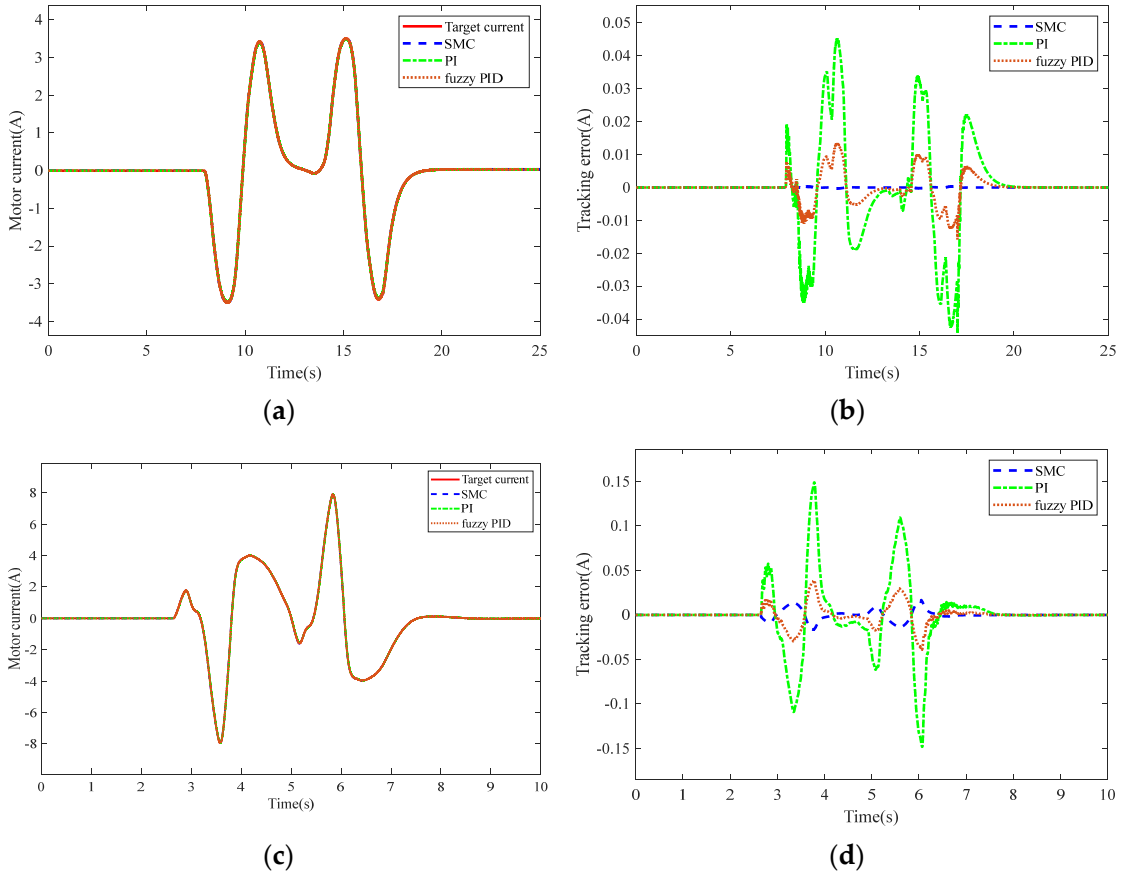


Figure 8. Controller control performance under double lane change condition: (**a**) Current tracking effect at 30 km; (**b**) Current error at 30 km; (**c**) Current tracking effect at 80 km; (**d**) Current error at 80 km.

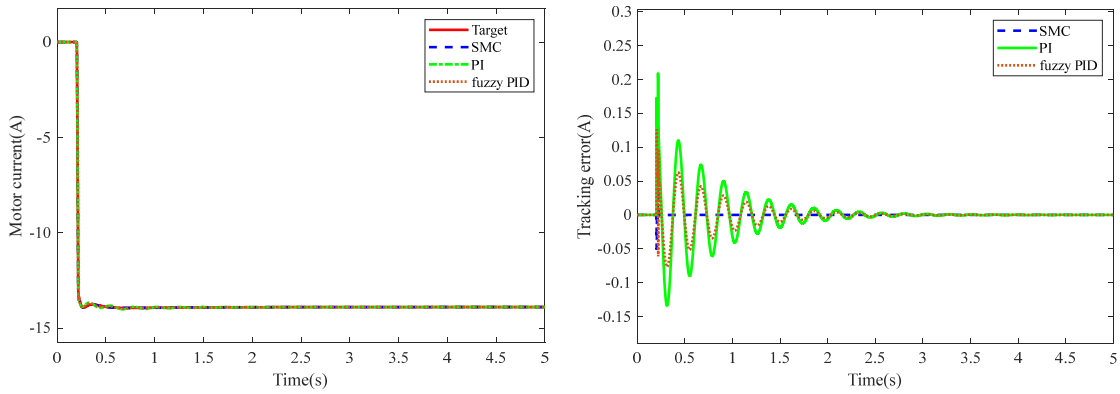
5.2. Step Test Conditions

The road adhesion coefficient is established at 0.85, and the vehicle speed is configured to 60 km/h, and a radian signal is input to the steering wheel to verify the performance of the controller under emergency maneuvering, and the simulation results are shown in Figure 9.

Then, we introduce a sinusoidal perturbation of 1 V in the motor voltage, which is an appropriate proportion of the disturbance compared to the input signal range of the system, and the antidisturbance effects of different control algorithms are shown in Figure 10.

From Table 5, it can be seen that the percentage of disturbance to the signal is 1.3% with PI control, which is a 55% reduction in the magnitude of disturbance compared to fuzzy PID. However, when sliding mode control is used, the sinusoidal perturbation has almost no effect on the system.

Table 5 shows the analysis of the simulation results under step conditions, which show that the road-sensing motor current under sliding mode control tracks well with shorter peak time and minimum overshoot.



(**a**) (**b**)

Figure 9. Control performance of different controllers under step conditions: (**a**) Current tracking effect; (**b**) Current error.

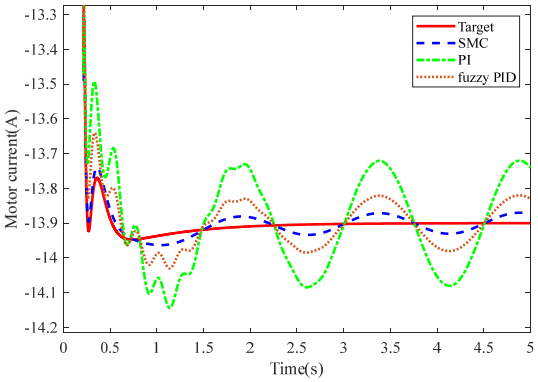


Figure 10. 1 V sinusoidal interference with different control algorithms.

Table 5. Step response performance index at 60 km/h.

Name	SMC	PI	Fuzzy PID
Rising time (s)	0.017	0.0175	0.037
Overshoot (%)	0.789	1.512	0.92
Steady value	−13.9	−13.9	−13.9

From Table 5, it can be seen that all three methods can achieve steady state, but the shortest peak time and the smallest amount of overshoot is achieved with sliding mode control.

6. Conclusions

In this paper, a road-sensing torque algorithm based on a nonlinear two-degree-of-freedom-vehicle model is designed for the SBW system in combination with an SMC. It can be seen that the designed road-sensing torque algorithm is effective and powerful for controlling the road-sensing motor current. The aim of this control strategy is to provide better road-sensing information for the driver's road safety. The main results are summarized below.

1. In the study of road sense simulation algorithms for steer-by-wire, the mainstream three methods include the use of sensors, the establishment of dynamics models, and parameter fitting. Compared with the other two methods, the road sense simulation algorithm proposed in this paper is built on the basis of a nonlinear two-degree-of-freedom vehicle model derived from the Magic Formula, with the addi-

tion of the return torque, damping torque, and friction torque, and the accuracy of the model is verified using the Carsim/Simulink co-simulation method. Post-validation, the algorithm enhances response and accelerates convergence, and the maximum steering wheel moment is slightly reduced, thus providing a robust basis for road-sensing simulations.

2. This study mainly focuses on the current control strategy of the road-sensing analogue motor and utilizes the sliding mode control method to improve the tracking performance of the current. Through the joint simulation, the sliding mode control controller is compared with PI controller and fuzzy PID controller, and the simulation results show that the designed sliding mode control controller still has good tracking effect at different speeds and under different working conditions, and the overshoot is smaller than both, which can better satisfy the real-time control requirements of the line steering road-sensing simulation.

In future research, we aim to enhance the road-sensing torque by considering the driver's style and optimizing it based on the road surface adhesion coefficient. Concurrently, we will develop a more precise system model and perform semi-physical simulations to further verify the practicality of the control strategy.

Author Contributions: Methodology, S.H.; software, K.A.; formal analysis, Z.A.Z.; resources, Y.Q.; data curation, Q.X.; writing—original draft preparation, K.A.; writing—review and editing, Y.Q.; project administration, K.A.; funding acquisition, S.H. All authors have read and agreed to the published version of the manuscript.

Funding: This research was funded by the National Natural Science Foundation of China (51875494), the Natural Science Research Program of Jiangsu Province Colleges and Universities (19KJB580019), and the Jiangsu Normal University Graduate Innovation Program Project (SJCX20_1353).

Data Availability Statement: The data that support the findings of this study are available from the corresponding author upon reasonable request. The data are not publicly available due to privacy concerns.

Conflicts of Interest: The authors declare no conflicts of interest.

References

1. Mortazavizadeh, S.A.; Ghaderi, A.; Ebrahimi, M.; Hajian, M. Recent Developments in the Vehicle Steer-by-Wire System. *IEEE Trans. Transp. Electrif.* **2020**, *6*, 1226–1235. [CrossRef]
2. Yang, A.X.; Zang, Y.H.; Xu, L.L.; Li, L.Y.; Tan, D.P. A Systematic Review and Future Development of Automotive Chassis Control Technology. *Appl. Sci.* **2023**, *13*, 11859. [CrossRef]
3. Fankem, S.; Müller, S. A new model to compute the desired steering torque for steer-by-wire vehicles and driving simulators. *Veh. Syst. Dyn.* **2014**, *52*, 251–271. [CrossRef]
4. Kirli, A.; Arslan, M.S. Online optimized hysteresis-based steering feel model for steer-by-wire systems. *Adv. Mech. Eng.* **2016**, *8*, 15. [CrossRef]
5. Cheon, D.; Nam, K.; Oh, S. Design and Robust Control of a Precise Torque Controllable Steering Module for Steer-by-Wire Systems. *IEEE Trans. Ind. Electron.* **2022**, *69*, 13245–13254. [CrossRef]
6. Zhang, H.; Wang, Y.Y.; Zhang, G.W.; Tang, C.H. Research on LADRC strategy of PMSM for road-sensing simulation based on differential evolution algorithm. *J. Power Electron.* **2020**, *20*, 958–970. [CrossRef]
7. Gholami, A.; Majidi, M. Development of a neuromuscular driver model with an estimation of steering torque feedback in vehicle steer-by-wire systems. *Proc. Inst. Mech Eng Pt K-J. Multi-Body Dyn.* **2019**, *233*, 657–667. [CrossRef]
8. Van Ende, K.T.R.; Schaare, D.; Kaste, J.; Küçükay, F.; Henze, R.; Kallmeyer, F.K. Practicability study on the suitability of artificial, neural networks for the approximation of unknown steering torques. *Veh. Syst. Dyn.* **2016**, *54*, 1362–1383. [CrossRef]
9. Liang, X.T.; Zhao, L.F.; Wang, Q.D.; Chen, W.W.; Xia, G.; Hu, J.F.; Jiang, P.F. A novel steering-by-wire system with road sense adaptive friction compensation. *Mech. Syst. Signal Proc.* **2022**, *169*, 19. [CrossRef]
10. Liang, W.H.; Zhao, W.Z.; Wang, C.Y.; Zou, S.C. Harmonic suppression and road feeling control of steer-by-wire system with permanent magnet synchronous motor. *Mech. Syst. Signal Proc.* **2022**, *172*, 19. [CrossRef]

11. Yu, L.Y.; Hu, Z.H.; Cai, Y.P.; Hou, Z.Y.; Shi, Y.J.; Wu, B.G.; Tian, M.L. Road Feel Simulation Method with Rack Force Observer for Intelligent Vehicle Steer-by-Wire System. *Int. J. Automot. Technol.* **2024**, 1–14, *Early Access*. [CrossRef]
12. Aly, M.; Roman, M.; Rabie, M.; Shaaban, S. Observer-Based Optimal Position Control for Electrohydraulic Steer-by-Wire System Using Gray-Box System Identified Model. *J. Dyn. Syst. Meas. Control-Trans. ASME* **2017**, *139*, 9. [CrossRef]
13. Sun, Z.; Zheng, J.C.; Man, Z.H.; Wang, H. Robust Control of a Vehicle Steer-by-Wire System Using Adaptive Sliding Mode. *IEEE Trans. Ind. Electron.* **2016**, *63*, 2251–2262. [CrossRef]
14. Ye, M.; Wang, H. Robust adaptive integral terminal sliding mode control for steer-by-wire systems based on extreme learning machine. *Comput. Electr. Eng.* **2020**, *86*, 16. [CrossRef]
15. Wang, H.; Xu, Z.M.; Do, M.T.; Zheng, J.C.; Cao, Z.W.; Xie, L.S. Neural-network-based robust control for steer-by-wire systems with uncertain dynamics. *Neural Comput. Appl.* **2015**, *26*, 1575–1586. [CrossRef]
16. Wang, H.; He, P.; Yu, M.; Liu, L.F.; Do, M.T.; Kong, H.F.; Man, Z.H. Adaptive neural network sliding mode control for steer-by-wire-based vehicle stability control. *J. Intell. Fuzzy Syst.* **2016**, *31*, 885–902. [CrossRef]
17. Liu, Y.C.; Wang, X.Y.; Zhang, G.W.; Yuan, Q.; Chen, Z.T.; Li, L. Road Sense Construction for Steer-by-Wire System: Data-Driven Feedback Torque Design and Friction Compensated Explicit Model Predictive Control. *IEEE Trans. Transp. Electrif.* **2024**, *10*, 9918–9930. [CrossRef]
18. Chen, Y. Research on force Feedback Control. Master's Thesis, Harbin Institute of Technology, Harbin, China, May 2010.
19. Hang, P.; Chen, X.B.; Fang, S.D.; Luo, F.M. Robust control for four-wheel-independent-steering electric vehicle with steer-by-wire system. Int. *J. Automot. Technol.* **2017**, *18*, 785–797. [CrossRef]
20. Lee, J.; Yi, K.; Lee, D.; Jang, B.; Kim, M.; Hwang, S. Haptic control of steer-by-wire systems for tracking of target steering feedback torque. *Proc. Inst. Mech. Eng. Part D-J. Automob. Eng.* **2020**, *234*, 1389–1401. [CrossRef]
21. Lee, S.; Lee, Y.; Jeong, H.; Lee, M. A Study on the Steering Force Feedback Control of the Steer by Wire System Using HiLS. *Trans. KSAE* **2021**, *29*, 49–56. [CrossRef]
22. Su, C.R.; Li, H.H.; Qiao, B.J.; Wu, X.D. Personalized Steering Feel Design for Steer-by-Wire Systems Based on the Rack Force Estimation. *Int. J. Automot. Technol.* **2023**, *24*, 1151–1161. [CrossRef]
23. Zhang, Q.Y.; Lin, W.P.; Wang, Y.R.; Wu, X.J.; Luo, Y.J. Control Strategy of the Vehicle's Active Steer by Wire. *J. Coast. Res.* **2020**, *103*, 355–360. [CrossRef]
24. Woo, S.; Heo, C.; Jeong, M.O.; Lee, J.M. Integral Analysis of a Vehicle and Electric Power Steering Logic for Improving Steering Feel Performance. *Appl. Sci.* **2023**, *13*, 11598. [CrossRef]
25. Kim, K.; Lee, J.; Kim, M.; Yi, K. Adaptive Sliding Mode Control of Rack Position Tracking System for Steer-by-Wire Vehicles. *IEEE Access* **2020**, *8*, 163483–163500. [CrossRef]
26. Alagappan, A.V.; Rao, K.V.N.; Kumar, R.K. A comparison of various algorithms to extract Magic Formula tyre model coefficients for vehicle dynamics simulations. *Veh. Syst. Dyn.* **2015**, *53*, 154–178. [CrossRef]
27. Zhao, X.P.; Li, X.; Chen, J.; Men, J.L. Parametric design and application of steering characteristic curve in control for electric power steering. *Mechatronics* **2009**, *19*, 905–911. [CrossRef]
28. Yang, H.H.; Liu, W.T.; Chen, L.; Yu, F. An adaptive hierarchical control approach of vehicle handling stability improvement based on Steer-by-Wire Systems. *Mechatronics* **2021**, *77*, 11. [CrossRef]
29. Zhang, J.; Wang, H.; Zheng, J.C.; Cao, Z.W.; Man, Z.H.; Yu, M.; Chen, L. Adaptive Sliding Mode-Based Lateral Stability Control of Steer-by-Wire Vehicles With Experimental Validations. *IEEE Trans. Veh. Technol.* **2020**, *69*, 9589–9600. [CrossRef]

Disclaimer/Publisher's Note: The statements, opinions and data contained in all publications are solely those of the individual author(s) and contributor(s) and not of MDPI and/or the editor(s). MDPI and/or the editor(s) disclaim responsibility for any injury to people or property resulting from any ideas, methods, instructions or products referred to in the content.